

Self-induced growth of vertical free-standing InAs nanowires on Si(111) by molecular beam epitaxy

This article has been downloaded from IOPscience. Please scroll down to see the full text article.

2010 Nanotechnology 21 365602

(<http://iopscience.iop.org/0957-4484/21/36/365602>)

View [the table of contents for this issue](#), or go to the [journal homepage](#) for more

Download details:

IP Address: 129.187.254.46

The article was downloaded on 22/11/2010 at 13:38

Please note that [terms and conditions apply](#).

Self-induced growth of vertical free-standing InAs nanowires on Si(111) by molecular beam epitaxy

G Koblmüller^{1,3}, S Hertenberger¹, K Vizbaras¹, M Bichler¹, F Bao², J-P Zhang² and G Abstreiter¹

¹ Walter Schottky Institut and Physik Department, Technische Universität München, 85748 Garching, Germany

² Suzhou Institute of Nano-Tech and Nano-Bionics, Chinese Academy of Sciences, 215125 Suzhou, People's Republic of China

E-mail: Gregor.Koblmuller@wsi.tum.de

Received 14 May 2010, in final form 14 July 2010

Published 12 August 2010

Online at stacks.iop.org/Nano/21/365602

Abstract

We report self-induced growth of vertically aligned (i.e. along the [111] direction), free-standing InAs nanowires on Si(111) substrates by solid-source molecular beam epitaxy. Implementation of an ultrathin amorphous SiO_x mask on Si(111) facilitated epitaxial InAs nanowire growth, as confirmed by high-resolution x-ray diffraction 2θ - ω scans and transmission electron microscopy. Depending on growth temperature (in the range of 400–520 °C) substantial size variation of both nanowire length and diameter was found under preservation of uniform, non-tapered hexagon-shaped geometries. The majority of InAs nanowires exhibited phase-pure zinc blende crystal structure with few defective regions consisting of stacking faults. Photoluminescence spectroscopy at 20 K revealed peak emission of the InAs nanowires at 0.445 eV, which is \sim 30 meV blueshifted with respect to the emission of the bulk InAs reference due to radial quantum confinement effects. These results show a promising route towards integration of well-aligned, high structural quality InAs-based nanowires with the desired aspect ratio and tailored emission wavelengths on an Si platform.

1. Introduction

Over the years, indium arsenide (InAs) has emerged as a high-performance narrow-bandgap semiconductor (bandgap energy $E_g \sim 0.36$ eV) with small electron effective mass, very high electron mobility ($>20\,000$ cm² V⁻¹ s⁻¹ at 300 K) and unique electro-optical properties [1]. These unique physical characteristics have made InAs an ideal electron confinement material in quantum wells [2] and quantum dots [3, 4], enabling superior performance in high-speed electronic and near-infrared (IR) optoelectronic applications [5, 6].

Concurrent with future flexibility and cost-effectiveness in device fabrication, monolithic integration of high-quality InAs-based materials with silicon (Si) has remained a long-sought vision in semiconductor technology. However, this has been hampered by large epitaxial strains and defect densities

arising from the significant crystal lattice mismatch (\sim 11.6% for InAs on Si) [7]. Implementation of free-standing III–V compound semiconductor nanowires on Si substrates via the vapor–liquid–solid (VLS) growth method was recently demonstrated as one of the most promising routes [8, 9] to allow very efficient strain accommodation and reduce critical lattice matching requirements [10, 11]. A number of reports have successfully shown free-standing epitaxial InAs nanowires on an Si substrate, mostly grown by metal–organic chemical vapor deposition (MOCVD) either with [12, 13] or without [13–15] the use of gold (Au) catalyst or by means of self-assembled organic coatings [16].

Simultaneously, solid-source molecular beam epitaxy (MBE) evolved as a powerful method to grow arsenide-based semiconductor nanowires with several interesting features, i.e. strongly non-equilibrium conditions allowing growth at lower substrate temperatures and low impurity incorporation due to an ultrahigh vacuum environment and

³ Author to whom any correspondence should be addressed.

pure elemental growth species. MBE also provides good interface, composition and doping control at the sub-monolayer level via exploitation of very low growth rates and sophisticated *in situ* growth control techniques [17–21]. The anticipated low impurity features are further expected to play a significant role for future ultrapure arsenide nanowire-based electronic devices on Si. Despite these promises, only a few attempts were aimed at epitaxial growth of free-standing InAs nanowires on Si by MBE [22–24], which were restricted to undesired Au catalyst-assisted conditions and reported difficulties in achieving vertically aligned [111]-oriented InAs nanowires [22]. Moreover, optical investigations to determine the bandgap energy of as-grown free-standing InAs nanowires have been rare and were mostly limited to either composition-dependent studies, i.e. of InAs_{1-x}P_x ternary compounds [25] or more complex InAs-core–InP-shell heterostructures [26]. The resulting emission spectra in these reports were based on dominant wurtzite (WZ) crystal structure in the InAs nanowires and were relying on strain effects at the core–shell interfaces. Hence, the optical properties from predominantly zinc blende (ZB) uncapped free-standing InAs nanowires still need to be demonstrated.

In this work, we developed self-induced growth (i.e. without the use of a foreign catalyst) of vertically well-oriented, free-standing InAs nanowires on Si(111) substrates by solid-source MBE. Specifically, the introduction of an ultrathin amorphous SiO_x mask on Si(111) facilitated epitaxial InAs nanowire growth, as demonstrated by detailed microstructural characterization using scanning electron microscopy (SEM), high-resolution x-ray diffraction (HRXRD) and transmission electron microscopy (HR-TEM). In addition, we also analyzed the emission spectra by low-temperature photoluminescence (PL) and demonstrated radial quantum confinement effects of as-grown, uncapped and predominantly zinc blende InAs nanowires. Given these results and the inherent advantages of the MBE method, the current work provides a profound basis for integration of InAs nanowire-based near-IR photonic devices of well-defined emission wavelengths with Si technology.

2. Experimental details

As substrates we used commercially available doped (n- or p-type), single-side polished Si(111) grown by the floating-zone technique. Prior to nanowire growth ~25–45 nm thick amorphous SiO_x was sputter-deposited on the epi-ready side of the Si(111) substrates. Subsequently, the SiO_x-coated substrates were selectively etched in an aqueous hydrofluoric (HF) acid solution (ratio of 1 HF (9%):2.5 H₂O), reducing the SiO_x thickness to a final thickness of ~2.5–6 nm as confirmed by spectroscopic ellipsometry. Amorphous SiO_x masks (either as native oxides or intentionally deposited) of similar thicknesses have previously been employed on InP [15], Si(111) [27] and GaAs [21, 28] substrates for nucleation of epitaxial III–V-based nanowires.

All growths were performed in a Gen-II MBE system equipped with standard effusion cells for group III elements and a Veeco valve cracker cell supplying arsenic (As₄). A pyrometer was used to measure the substrate temperature

in situ, which was calibrated to the onset temperature for desorption of the (001) GaAs surface native oxide. The supplied fluxes are expressed in equivalent (111) InAs thin film growth rate units (Å s⁻¹), as measured by reflection high energy electron diffraction (RHEED) during group-III-limited and As-limited growth experiments at temperatures of negligible thermal decomposition. For conversion to a.u., we note that in zinc blende InAs $a/2 = 3.4 \text{ \AA}$ refers to 1 monolayer (ML) along the [111] direction.

Upon loading the samples into the MBE chamber, the SiO_x-coated substrates were first annealed in an As₄ flux of 1.51 Å s⁻¹ (i.e. beam equivalent pressure (BEP) of 2.6×10^{-6} mbar) for 20 min at 760 °C to remove any contaminants. After the subsequent cool-down to typical InAs growth temperatures in the range of ~400–520 °C, nanowire growths were performed for 45 min using the same As flux as noted above and an In flux of ~0.26 Å s⁻¹. This corresponds to an In/As flux ratio of ~0.17, i.e. heavy As-rich growth conditions. Growth was terminated by switching off the In supply while maintaining the As₄ supply until the substrate temperature dropped to below 300 °C.

3. Results and discussion

Representative scanning electron microscopy (SEM) images of typical InAs nanowires are shown in figure 1 for two distinct growth temperatures of (a) 430 °C and (b) 505 °C. Obviously, the InAs nanowires exhibit predominant vertical directionality related to the {111} family of orientations, indicating a direct relationship to the underlying Si(111) substrate. For the majority of the nanowires their nucleation occurred directly at the interface to the substrate surface, resulting in fairly straight non-tapered nanowires with hexagon-shaped geometries (see both insets and top-view SEM images at the bottom of figures 1(a) and (b)). According to recent observations of [111]-oriented group III As-based nanowires with hexagonal geometry, their six sidewall facets are expected to correspond to the {110} family of orientations [29]. Although no droplets related to a group III element (i.e. In)-rich phase could be resolved at the individual nanowire tips by SEM, their existence could be anticipated during growth to govern nucleation and condensation via the vapor–liquid–solid (VLS) mechanism, as common in typical self-catalyzed MBE-grown group III As-based nanowires [28]. In this case, the disappearance of the metallic In droplets may be related to their consumption and crystallization by excess As₄ during post-growth cooling. However, ongoing experiments based on *in situ* RHEED studies are expected to resolve this in more detail and will be published in a separate paper.

Top-view SEM imaging yielded furthermore InAs nanowire densities in the range of ~1–2 × 10⁹ cm⁻² over the investigated temperature range. In contrast to the negligible variation in nanowire densities, we observed more significant variation in nanowire length and diameter with substrate temperature. As shown in figure 1(c), for fixed growth time (45 min) the nanowire length reached peak values of ~700–900 nm between 430 and 460 °C and dropped on the low- and high-temperature sides to values

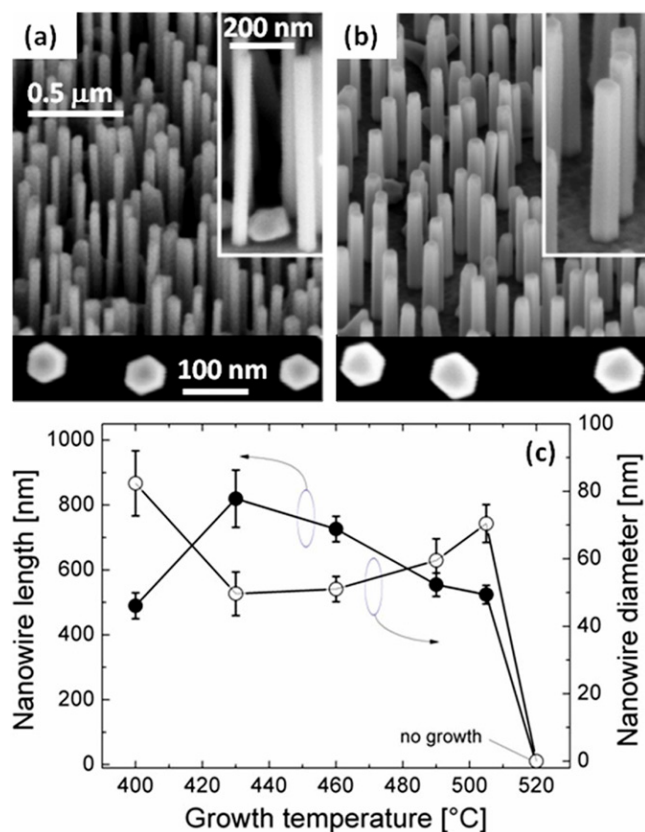


Figure 1. Scanning electron micrographs of InAs nanowires grown on Si(111) at temperatures of (a) 430 °C and (b) 505 °C. Magnified areas (insets) and top-view images (bottom) show the nanowire/substrate interface and hexagonal geometry, respectively. (c) Corresponding length/diameter versus growth temperature plot for a range of temperatures from 400 to 520 °C (error bars were determined from measuring approximately 30 nanowires at each temperature.)

below ~ 600 nm. It is important to note that no nanowire growth was achieved at the highest growth temperature of 520 °C. The observation of peak nanowire lengths within a certain temperature region implies a general trend also observed for MOCVD-grown InAs nanowires [15, 16]. In the present study, the maximum nanowire lengths were, however, achieved at approximately ~ 100 – 150 °C lower growth temperatures (as compared to [15, 16]), mainly because in MBE processes the impinging growth species do not require activation and dissociation at the growth surface. Moreover, we attribute the decreased lengths and growth inhibition at the high-temperature end (460–520 °C) to the increased thermal decomposition rates along the InAs(111) growth direction [30]. On the other hand, the decreased nanowire length at lower growth temperatures (< 430 °C) can be explained by the reduced diffusion lengths of adatoms and hence their decreased incorporation probability at the nanowire tip, limiting growth along the vertical direction. Both these vertical-growth-restricting effects at the low- and high-temperature ends are directly reflected by increased nanowire diameters (~ 65 – 90 nm) (figure 1(c)). In contrast, smaller diameters of ~ 40 – 65 nm associated with substantially longer nanowires were observed in the intermediate temperature range. This inverse length/diameter dependence ($L \sim 1/D$)

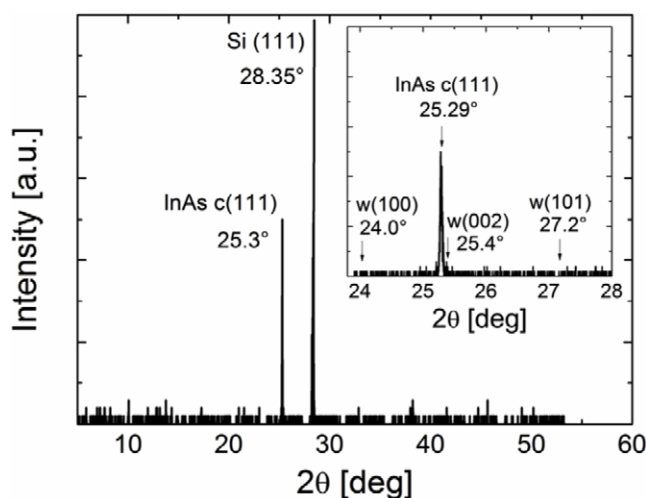


Figure 2. XRD 2θ - ω scan of representative InAs nanowire sample (grown at 460 °C) illustrating two peaks associated with zinc blende (111) InAs (25.3°) and (111) Si substrate (28.35°). The inset shows a high-resolution scan in the vicinity of the zinc blende (111) InAs peak for identification of possible additional peaks related to wurtzite crystal phase.

was also reported for a number of nanowire and whisker-like systems, e.g. for Si whiskers [31] and GaAs nanowires [32]. Such form of $L(D)$ dependence is characteristic of diffusion-limited growth of wire-like crystals that was investigated theoretically and experimentally by Sears [33], Dittmar and Neumann [34], and Dubrovskii *et al* [32]. Thus, in the diffusion-limited growth regime (i.e. where nanowire growth proceeds via adatom diffusion along the side facets to the nanowire tip), the observed $L(D)$ dependence is anticipated to apply generally for any material system and may further be independent of the specific growth method.

To confirm the structural quality between the InAs nanowires and the Si(111) substrate out-of-plane symmetric HRXRD 2θ - ω scans in a Philips Xpert MRD diffractometer were performed on selected nanowire samples. As shown for the sample grown at 460 °C, only two characteristic peaks were identified over a wide 2θ range (0° – 60°), with their positions corresponding to zinc blende (ZB) InAs(111) at 25.3° (lattice constant $a = 0.6058$ nm) and Si(111) at 28.35° (figure 2). This demonstrates the overall phase purity of the grown InAs nanowires and further provides the direct epitaxial relationship, i.e. InAs[111] \parallel Si[111]. Additional 2θ - ω scans were performed in high resolution over a narrower range (24° – 28°) to identify any possible wurtzite (WZ) phases in the vicinity of the dominant ZB peak at 25.3° (magnified inset of figure 2). The WZ phases with lowest-order Miller indices and highest intensity typically occur at 2θ angles of 24° (for 100), 25.4° (for 002) and 27.2° (for 101), where $a = 0.4274$ nm and $c = 0.702$ nm [35]. Although these WZ peaks were occasionally seen in HRXRD 2θ - ω scans of MBE-grown III-V-based nanowires on Si(111) [19], they could not be resolved in our current InAs nanowire arrays. The presence of WZ phases in predominant ZB nanowires is generally related to high densities of stacking faults (SFs), i.e. alternating crystal structure changes from ZB to WZ along the growth direction [35].

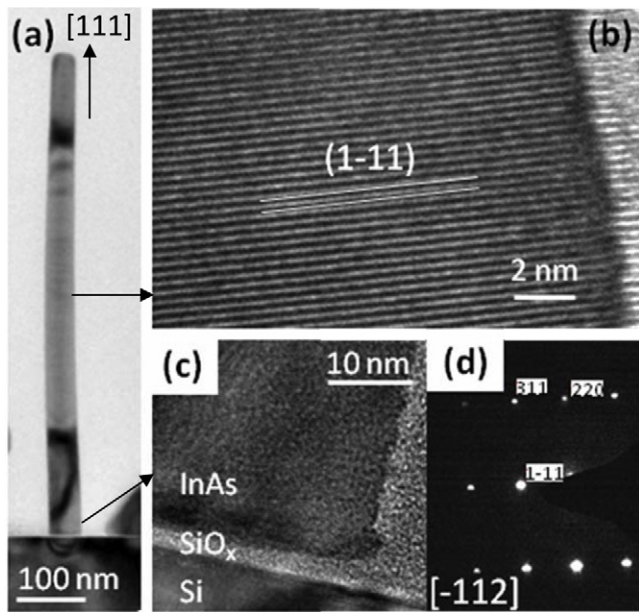


Figure 3. Cross-section TEM images of a typical InAs nanowire nucleated on Si(111) (460 °C sample) presented in (a) low magnification and (b) high resolution in the near-center region and (c) at the bottom nanowire/substrate interface. (d) SAED pattern along the $[\bar{1}12]$ direction showing preferential $[111]$ nanowire growth orientation.

More insights into the crystal structure of the InAs nanowires were provided by TEM analysis (figure 3) using an FEI Tecnai FEG microscope operated at 200 kV. The bright-field low-magnification TEM image in figure 3(a) shows a representative InAs nanowire as grown on an Si(111) substrate (sample grown at 460 °C). This image also demonstrates that the diameter of the nanowire is uniform along its entire length and that the nanowire grew along the $[111]$ direction. The latter was also confirmed by the selected-area electron diffraction pattern (SAED) recorded along the $[\bar{1}12]$ direction (figure 3(d)). Further high-resolution TEM analysis in the near-center region of the same nanowire revealed the individual ZB atomic $(1\bar{1}1)$ planes, with an interplanar spacing of 0.34 nm along the nanowire growth direction that corresponds well to that of bulk InAs (figure 3(b)). Figure 3(c) shows another HR-TEM image of the nanowire/substrate interface, showing nucleation of the InAs nanowire at the amorphous ~ 3 nm thick SiO_x mask layer. We note that occasionally an individual nanowire was also identified which was slightly tilted (i.e. $<10^\circ$) against the vertical $[111]$ direction. Such a nanowire showed alternating dark and bright contrast stripes in specific regions of low-magnification TEM micrographs. Corresponding HR-TEM image and SAED pattern related these stripes to defective regions with high densities of WZ/ZB SFs (not shown). Nevertheless, their occurrence was rather low, mimicking low SF density GaAs nanowires grown under similar As-rich growth conditions [36], which further explains the limited signal of WZ phases in the HRXRD measurements of figure 2.

Finally, low-temperature (20 K) photoluminescence (PL) spectra using an excitation laser wavelength of 808 nm were

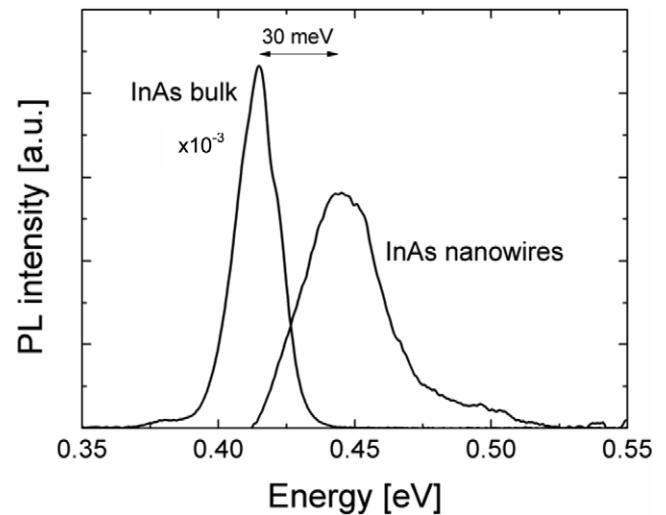


Figure 4. 20 K photoluminescence spectra at 250 mW excitation power of InAs nanowire array (sample grown at 460 °C) as compared to bulk InAs reference.

recorded on an InAs nanowire array with an average diameter of ~ 50 nm (sample grown at 460 °C) in comparison with the bulk InAs reference (figure 4). The dominant PL peak emission of the InAs nanowire array was at 0.445 eV with a full width at half-maximum (FWHM) of ~ 33 meV. On the high energy side of this PL peak a shoulder appeared at around 0.50 eV, which might have arisen from band transitions associated with occasional WZ segments. Note that this ~ 55 meV peak shift with respect to the dominant PL peak corresponds well to a theoretically calculated bandgap increase from ZB to WZ InAs [37]. Moreover, the peak emission energies for both the ZB and WZ phases are lower than those extrapolated for WZ InAs from bandgap measurements of ternary InAsP compound nanowires [26]. On the other hand, the dominant (ZB) PL peak in figure 4 was also slightly blueshifted by ~ 30 meV with respect to bulk InAs. This reflects the anticipated radial quantum confinement effects, as will be elucidated in a forthcoming paper based on systematic nanowire size-dependent studies using power-dependent PL peak emission shifts.

4. Conclusions

In summary, we demonstrated self-induced free-standing InAs nanowires grown by solid-source MBE on Si(111) using an ultrathin amorphous SiO_x mask. Significant size variation (diameter/length) was achieved by control of growth temperature between 400 and 520 °C. Detailed microstructural analysis revealed overall well-oriented (i.e. $[111]$) nanowires with phase-pure zinc blende crystal structure, with a few exceptions of nanowires showing defective regions of WZ/ZB-related stacking faults. The PL peak emission was found at 0.445 eV and was slightly blueshifted from bulk InAs, highlighting the differences arising from quantum-size geometry effects. These results pave the way for integration of high-quality MBE-grown InAs nanowires with Si technology.

Acknowledgments

We kindly thank S Lindner, E Forster and F Herzog for enduring SEM measurements and A W Holleitner and P Weiser for support. We gratefully acknowledge D Spirkoska and A Fontcuberta i Morral (EPFL Lausanne) for many helpful discussions. The main author also thanks M Stutzmann for providing the XRD facilities. This work was supported by the Marie Curie FP7 Reintegration Grant (Christina Totté, program manager), the DFG excellence program Nanosystems Initiative Munich and the collaborative research center SFB 631.

References

- [1] Milnes A G and Polyakov A Y 1993 *Mater. Sci. Eng. B* **18** 237
- [2] Akazaki T, Nitta J, Takayanagi H, Enoki T and Arai K 1994 *Appl. Phys. Lett.* **65** 1263
- [3] Medeiros-Ribeiro G, Leonhard D and Petroff P M 1995 *Appl. Phys. Lett.* **66** 1767
- [4] Chu L, Arzberger M, Böhm G and Abstreiter G 1999 *J. Appl. Phys.* **85** 2355
- [5] Bolognesi C R, Caine E J and Kroemer H 1994 *IEEE Electron Device Lett.* **15** 16
- [6] Zhukov A E et al 1999 *IEEE Photon. Technol. Lett.* **11** 1345
- [7] Grober R D, Drew H D, Chyi J-I, Kalem S and Morkoc H 1989 *J. Appl. Phys.* **65** 4079
- [8] Mårtensson T, Svensson C P T, Wacaser B A, Larsson M W, Seifert W, Deppert K, Gustafsson A, Wallenberg L R and Samuelson L 2004 *Nano Lett.* **5** 457
- [9] Roest A L, Verheijen M A, Wunnicke O, Serafin S, Wondergem H and Bakkers E P A M 2006 *Nanotechnology* **17** 271
- [10] Glas F 2006 *Phys. Rev. B* **74** 121302
- [11] Chuang L C, Moewe M, Chase C, Kobayashi N P, Chang-Hasnain C and Crankshaw S 2007 *Appl. Phys. Lett.* **90** 043115
- [12] Roddaro S et al 2009 *Nanotechnology* **20** 285303
- [13] Dayeh S A, Yu E T and Wang D 2007 *J. Phys. Chem. C* **111** 13331
- [14] Tomioka K, Motohisa J, Hara S and Fukui T 2008 *Nano Lett.* **8** 3475
- [15] Mandl B, Stangl J, Mårtensson T, Mikkelsen A, Eriksson J, Karlsson L S, Bauer G, Samuelson L and Seifert W 2006 *Nano Lett.* **6** 1817
- [16] Mårtensson T et al 2007 *Adv. Mater.* **19** 1801
- [17] Wu Z H, Sun M, Mei X Y and Ruda H E 2004 *Appl. Phys. Lett.* **85** 657
- [18] Lugstein A, Andrews A M, Steinmair M, Hyun Y J, Bertagnonli E, Weil M, Pongratz P, Schrambock M, Roch T and Strasser G 2007 *Nanotechnology* **18** 35306
- [19] Ihn S G, Song J I, Kim Y H, Lee J Y and Ahn I H 2007 *IEEE Trans. Nanotechnol.* **6** 384
- [20] Fontcuberta i Morral A, Spirkoska D, Arbiol J, Heigoldt M, Morante J R and Abstreiter G 2008 *Small* **4** 899
- [21] Colombo C, Spirkoska D, Frimmer M, Abstreiter G and Fontcuberta i Morral A 2008 *Phys. Rev. B* **77** 155326
- [22] Ihn S G and Song J I 2007 *Nanotechnology* **18** 355603
- [23] Sorensen B S, Aagesen M, Sorensen C B, Lindelof P E, Martinez K L and Nygard J 2008 *Appl. Phys. Lett.* **92** 012119
- [24] Cirlin G E, Dubrovski V G, Soshnikov I P, Sibirev N V, Samsonenko Y B, Bouravlev A D, Harmand J C and Glas F 2009 *Phys. Status Solidi (RRL)* **3** 112
- [25] Tragardh J, Persson A I, Wagner J B, Hessmann D and Samuelson L 2007 *J. Appl. Phys.* **101** 123701
- [26] Zanolli Z, Pistol M E, Froberg L E and Samuelson L 2007 *J. Phys.: Condens. Matter* **19** 295219
- [27] Mattila M, Hakkarainen T, Lipsanen H, Jiang H and Kauppinen E I 2006 *Appl. Phys. Lett.* **89** 063119
- [28] Fontcuberta i Morral A, Colombo C, Abstreiter G, Arbiol J and Morante J R 2008 *Appl. Phys. Lett.* **92** 063112
- [29] Zardo I, Conesa-Boj S, Peiro F, Morante J R, Arbiol J, Uccelli E, Abstreiter G and Fontcuberta i Morral A 2009 *Phys. Rev. B* **80** 245324
- [30] Hooper S E, Westwood D I, Woolf D A, Heghoyan S S and Williams R H 1993 *Semicond. Sci. Technol.* **8** 1069
- [31] Schubert L, Werner P, Zakharov N D, Gerth G, Kolb F M, Long L, Goesele U and Tan T Y 2004 *Appl. Phys. Lett.* **84** 4968
- [32] Dubrovskii V G, Cirlin G E, Soshnikov I P, Tonkikh A A, Sibirev N V, Samsonenko Yu B and Ustinov V M 2005 *Phys. Rev. B* **71** 205325 and references therein
- [33] Sears G W 1953 *Acta. Metall.* **1** 457
- [34] Dittmar W and Neumann K 1960 *Z. Elektrochem.* **64** 207
- [35] Takahashi K and Moriizumi T 1966 *Japan. J. Appl. Phys.* **5** 657
- [36] Spirkoska D et al 2009 *Phys. Rev. B* **80** 245325
- [37] Zanolli Z, Fuchs F, Furthmüller J, von Barth U and Bechstedt F 2007 *Phys. Rev. B* **75** 245121